Detecting undetectables: Can conductances of action potential models be changed without appreciable change in the transmembrane potential?

Cite as: Chaos **29**, 073102 (2019); https://doi.org/10.1063/1.5087629
Submitted: 03 January 2019 . Accepted: 12 June 2019 . Published Online: 02 July 2019

Karoline Horgmo Jæger, Samuel Wall, and Aslak Tveito

Detecting undetectables: Can conductances of action potential models be changed without appreciable change in the transmembrane potential?

Cite as: Chaos **29**, 073102 (2019); doi: 10.1063/1.5087629
Submitted: 3 January 2019 · Accepted: 12 June 2019 ·
Published Online: 2 July 2019

Karoline Horgmo Jæger,[1] Samuel Wall,[1] and Aslak Tveito[1,2]

AFFILIATIONS

[1]Simula Research Laboratory, 1325 Lysaker, Norway
[2]Department of Informatics, University of Oslo, 1072 Blindern, Norway

ABSTRACT

Mathematical models describing the dynamics of the cardiac action potential are of great value for understanding how changes to the system can disrupt the normal electrical activity of cells and tissue in the heart. However, to represent specific data, these models must be parameterized, and adjustment of the maximum conductances of the individual contributing ionic currents is a commonly used method. Here, we present a method for investigating the uniqueness of such resulting parameterizations. Our key question is: Can the maximum conductances of a model be changed without giving any appreciable changes in the action potential? If so, the model parameters are not unique and this poses a major problem in using the models to identify changes in parameters from data, for instance, to evaluate potential drug effects. We propose a method for evaluating this uniqueness, founded on the singular value decomposition of a matrix consisting of the individual ionic currents. Small singular values of this matrix signify lack of parameter uniqueness and we show that the conclusion from linear analysis of the matrix carries over to provide insight into the uniqueness of the parameters in the nonlinear case. Using numerical experiments, we quantify the identifiability of the maximum conductances of well-known models of the cardiac action potential. Furthermore, we show how the identifiability depends on the time step used in the observation of the currents, how the application of drugs may change identifiability, and, finally, how the stimulation protocol can be used to improve the identifiability of a model.

Excitable cells are present in the brain, in the heart, in every muscle, and in all critical organs of the body. The dynamics of such cells are surprisingly complex and are commonly studied using detailed mathematical models based on experimental measurements of underlying biophysical processes. However, such models continue to increase in complexity as more experimental data become available, and it becomes correspondingly more challenging to understand how the parameters of the model affect the solutions. In the present report, we investigate this problem in models describing cardiac cell dynamics. In particular, we ask: Can different model parameters give identical output? Answers to this question turn out to be highly important when we want to evaluate the effect of drugs in the cardiac system or if we want to characterize the effect of genetic mutations on system dynamics. Here, we use the singular value decomposition (SVD) to investigate if it is possible to change model parameters, in our case the maximum conductances of the major ion currents that drive the function of the cell, without seeing any discernible effects on the action potential (AP). We find that commonly used models of the action potential of human cardiac cells have this property such that significant changes in the parameters can be introduced without any resulting change in commonly measured system outputs.

I. INTRODUCTION

In a conversation with Enrico Fermi, John von Neumann famously said, "with four parameters I can fit an elephant, and with five I can make him wiggle his trunk."[1] Clearly, both Fermi and von Neumann were cautious in introducing new parameters in mathematical models of physics, because they feared that with large degrees

of freedom, the equations could basically be tweaked to fit any observation. Although mathematical models in biology historically have roots in physics, the frugality of classical models in physics has not translated well over to biology. This is particularly the case in recent mathematical models describing the dynamics of electrically active cardiac cells, where it is difficult even to count the number of adjustable parameters, let alone estimate all their values.

Since the seminal papers of Hodgkin and Huxley[2] and Noble,[3] mathematical models have been used extensively and successfully to understand the action potential (AP) of excitable cells. Recent years have witnessed a very strong growth in the number of models describing a wide variety of cells and behaviors; see, e.g., Ref. 4 for a comprehensive collection of models. Introduction to mathematical models of the AP is provided in Refs. 5–8 and review of recent developments of AP models for cardiac cells is presented in Refs. 9–13. Early models of cardiac cells were rather compact, in the sense that they were formulated in terms of relatively few ordinary differential equations, but recent models tend to be quite large. For small models, it is possible to understand the dynamics described by the model equations, but for large and complex models, it is increasingly hard to understand the dynamics represented by all the terms entering the model, and useful information concerning the output of the model must be based on numerical computations.

It has consequently become increasingly difficult to analyze the mapping between the model parameters and the solution, leading to significant challenges in parameterizing the models to reflect a given data set. Such a parametrization is commonly approached using a variety of techniques, from detailed analysis of individual contributing currents, to inheritance from previous work done in completely nonrelevant experiments.[14,15] A comprehensive list of challenges associated with the parameterization of AP models is given in Ref. 15; data from numerous sources are combined in a model and the final parametrization is usually done by hand tuning. Promising steps toward improving parametrization are presented in Ref. 15, but quality assessment of the final model is still called for.

Here, we will examine this problem by assuming that the action potential of a paced cell can be accurately measured and that the problem of parametrization is to adjust a given model to the acquired waveform using a specific stimulation protocol. This is particularly relevant for techniques where the transmembrane potential is measured optically using voltage sensitive fluorescence; see, e.g., Refs. 16 and 17. Such a voltage sensitive reporting is now routinely used to analyze many cells including human induced pluripotent stem cells (hiPSCs); see, e.g., Ref. 18. We have recently developed methods for inverting data representing the transmembrane potential and intracellular calcium concentration of hiPSC-derived cardiomyocytes; see Ref. 19. In that project, it turned out to be essential to be able to automatically invert measured data to obtain the maximum conductances of an AP model. Furthermore, it became clear that some currents could be identified using calcium and voltage data, whereas other membrane currents were practically invisible using this data.

The purpose of the present report is to present a method for investigating the identifiability of conductances based on observations of the transmembrane potential. Although AP models are defined by numerous parameters entering the components of the models, the maximum conductances are most commonly used for parameterization of new data; see, e.g., Refs. 14 and 15. The method is based on the singular value decomposition (SVD; see, e.g., Refs. 20 and 21) of a matrix representing the individual transmembrane ion currents, I_i. These ion currents contribute to the total transmembrane current,

$$I_T = \sum_{i=1}^{N} I_i, \tag{1}$$

and this total transmembrane current governs the dynamics of the cellular transmembrane potential, $v = v(t)$, by

$$\frac{dv(t)}{dt} = -I_T. \tag{2}$$

Here, we have chosen to formulate (2) so that the transmembrane currents are expressed as current per cell capacitance, given in units of Amperes per Farad (A/F), v is given in millivolts (mV) and time, t, is given in milliseconds (ms). Note, however, that (2) could alternatively be expressed as, for example, $C_m \frac{dv(t)}{dt} = -i_T$, where C_m is the specific cell capacitance (in μF/cm^2), i_T is the total transmembrane current density (in μA/cm^2), and v and t are given in mV and ms, respectively.

We are interested in estimating the effect of replacing an ion current I_i by a perturbed current given by $(1 + \lambda_i)I_i$. If the effect of such a perturbation is small, it will be very difficult to parameterize the current by simply observing changes in the total membrane current I_T given by (1). In order to investigate how changes in the membrane currents, I_i, affect the total current, I_T, we perform an AP simulation using the model (2). At given time steps in the simulation (e.g., every millisecond), we store the values of every ion current in a matrix A; each row in the matrix represents the individual ion currents at a given time step. Then, we compute the singular values and singular vectors of that matrix. If a singular value of the matrix is zero, it means that if we change the vector of conductances along the corresponding nonzero singular vector, the total current will not change and therefore no changes can be observed in the transmembrane potential.

However, linear analysis of the matrix containing the ion currents cannot directly be used to predict the effect of perturbations on the transmembrane potential. In fact, the original model reads

$$\frac{dv(t)}{dt} = -\sum_{i=1}^{N} I_i(v, s), \tag{3}$$

and the perturbed model reads

$$\frac{dv^\lambda(t)}{dt} = -\sum_{i=1}^{N} (1 + \lambda_i) I_i(v^\lambda, s^\lambda). \tag{4}$$

Here, s is a vector containing other state variables of the model. Therefore, the $(1 + \lambda_i)$ perturbation introduces a nonlinear perturbation and we describe below how the linear results translate into nonlinear effects.

The common way of investigating the sensitivity of nonlinear AP models of the form (1) is to compare the solutions of the model with and without perturbed conductances. When every individual conductance is analyzed, a rough indication of the parameter sensitivity is obtained; see, e.g., Refs. 19, 22–25. This method is well established and clearly provides valuable insight. However, the method

can only detect sensitivities for single currents and not combinations of currents. Suppose, for instance, that two currents are very sensitive when they are perturbed individually, but if both are increased, the changes cancel each other out and no discernible changes can be observed in the total membrane current. Such subtle cancelation effects turn out to be surprisingly common and almost (or perhaps entirely) impossible to see if only individual currents are perturbed. It is also very hard to search for such insensitivities by randomly combining various currents because the search space is so large and each simulation is time consuming. Therefore, the SVD method turns out to be useful and we will demonstrate how it works for well-known models of human ventricular APs.

II. METHODS

Our aim is to develop a method for investigating the uniqueness of the maximum conductances in AP models. The question we want to get at is this: For a given AP model and a specific stimulation protocol, can the maximum conductances be changed significantly without appreciable changes in the resulting transmembrane potential?

We will assume that the transmembrane potential is governed by a model of the form

$$\frac{dv(t)}{dt} = -\sum_{i=1}^{N} I_i(v,s), \tag{5}$$

$$\frac{ds(t)}{dt} = F(v,s). \tag{6}$$

Here, as above, v denotes the transmembrane potential, s denotes the other variables of the AP model (concentrations and gating variables), $\{I_i\}_{i=1}^N$ denotes the collection of ion currents, and F represents the dynamics of the gating variables and the ion concentrations. We assume that each ion current can, for example, be written in the form

$$I_i = g_i o_i (v - v_i^0), \tag{7}$$

where g_i denotes the maximum conductance, o_i is the open probability, and v_i^0 denotes the resting potential of the ith ion channel.

In addition to the model (5), we will also consider the following perturbed model:

$$\frac{dv^\lambda(t)}{dt} = -\sum_{i=1}^{N} (1+\lambda_i) I_i(v^\lambda, s^\lambda), \tag{8}$$

$$\frac{ds^\lambda(t)}{dt} = F(v^\lambda, s^\lambda; \lambda), \tag{9}$$

which is similar to the original model except that every ion current is perturbed by a term of the form $(1+\lambda_i)$. Clearly, $v = v^\lambda$ for $\lambda = 0$, but can we find a vector $\lambda \neq 0$ such that $v \approx v^\lambda$? If such a vector λ exists, then clearly knowing the values of the transmembrane potential for all points in time is not enough to infer the maximum conductances, because different maximum conductances can give the same transmembrane potential.

A. Recording currents during an AP simulation

During a simulation based on the model (5)–(6), we store the total membrane current and the individual ion currents at certain time steps. More precisely, we store the total membrane current I_T^k and the individual currents I_j^k for $j = 1,\dots,N$ at time $t_k = k\Delta t$ for $k = 1,..,M$. Here, N denotes the number of ion currents and M denotes the number of time steps at which the currents are stored. We are interested in the effect of perturbing individual currents and for that purpose we introduce the vector $\mu \in \mathbb{R}^{N,1}$. With $\mu = (1,1,\dots,1)^T$, we can write the total membrane current as a matrix-vector product,

$$I_T = A\mu, \tag{10}$$

where we have gathered all individual ion currents in the matrix A defined by

$$A = \begin{pmatrix} I_1^1 & \cdots & I_N^1 \\ \vdots & & \vdots \\ I_1^M & \cdots & I_N^M \end{pmatrix}, \tag{11}$$

and the total current is given by

$$I_T = \begin{pmatrix} I_T^1 \\ I_T^2 \\ \vdots \\ I_T^M \end{pmatrix}.$$

Note that

$$I_T \in \mathbb{R}^{M,1}, \quad A \in \mathbb{R}^{M,N}, \quad \text{and} \quad \mu \in \mathbb{R}^{N,1}.$$

In the equation $I_T = A\mu$, every column of the matrix A represents one of the ion currents recorded at every time step. These currents are multiplied by 1, and, thus, the row-sums become the total current for every time step. By perturbing μ, we can perturb the recorded currents and study the effect of this on the total current. If we can find perturbations to μ that do not change the total current, such a perturbation would be impossible to detect by observing the transmembrane potential. As we will see below, the SVD algorithm is well suited to study the effect of such perturbations.

B. The singular value decomposition (SVD) of the current matrix

The SVD exists for any matrix A and takes the form

$$A = USV^T; \tag{12}$$

see, e.g., Refs. 20 and 21. Here, $U \in \mathbb{R}^{M,M}$, $V \in \mathbb{R}^{N,N}$, and $S \in \mathbb{R}^{M,N}$. Note that U and V are unitary matrices, i.e.,

$$UU^T = I, \quad U^TU = I, \quad VV^T = I, \quad V^TV = I,$$

where I is the identity matrix. The matrix S is a diagonal matrix with positive singular values σ_i satisfying

$$\sigma_1 \geq \sigma_2 \geq \cdots \geq \sigma_r > 0,$$

where r is the rank of the matrix A. The singular values and singular vectors satisfy the following relations:

$$Av_i = \sigma_i u_i, \quad i = 1,\dots,r, \tag{13}$$

$$Av_i = 0, \quad i = r+1,\dots,N, \tag{14}$$

$$A^T u_i = \sigma_i v_i, \quad i = 1, \ldots, r, \tag{15}$$

$$A^T u_i = 0, \quad i = r+1, \ldots, M. \tag{16}$$

Furthermore, the singular vectors define orthonormal bases as follows:

$$\{u_1, \ldots, u_r\} \text{ is an orthonormal basis for } \mathcal{N}(A^T)^\perp, \tag{17}$$

$$\{u_{r+1}, \ldots, u_M\} \text{ is an orthonormal basis for } \mathcal{N}(A^T), \tag{18}$$

$$\{v_1, \ldots, v_r\} \text{ is an orthonormal basis for } \mathcal{N}(A)^\perp, \tag{19}$$

$$\{v_{r+1}, \ldots, v_N\} \text{ is an orthonormal basis for } \mathcal{N}(A). \tag{20}$$

Here, $\mathcal{N}(A)$ and $\mathcal{N}(A^T)$ are the null spaces of A and A^T, respectively, and $\mathcal{N}(A^T)^\perp$ and $\mathcal{N}(A)^\perp$ are the column and row spaces of A, respectively.

C. The effect of perturbing the parameter vector μ; the maximum conductances

We will use the SVD to analyze the effect of perturbing the parameter vector μ. For that purpose, recall that

$$I_T = A\mu,$$

and consider also the total membrane current for a perturbed vector, $\bar{\mu}$,

$$\bar{I}_T = A\bar{\mu}.$$

1. Perturbation along a singular vector

Let us first consider the special case of

$$\bar{\mu} = \mu + \varepsilon v_i,$$

where v_i is a singular vector of A [see (13)] and ε is a parameter indicating the strength of the perturbation (the Euclidian norm of v_i is one).

Note that

$$I_T - \bar{I}_T = A\mu - A\bar{\mu} = -\varepsilon A v_i = -\varepsilon \sigma_i u_i,$$

and, therefore, in the Euclidian norm $\|\cdot\|$ and the associated inner product $(\cdot,\cdot)$, we have

$$\|I_T - \bar{I}_T\|^2 = (I_T - \bar{I}_T, I_T - \bar{I}_T) = \varepsilon^2 \sigma_i^2 (u_i, u_i) = \varepsilon^2 \sigma_i^2,$$

so

$$\|I_T - \bar{I}_T\| = \varepsilon \sigma_i. \tag{21}$$

This means that the effect of a perturbation along a singular vector is proportional to the associated singular value. Therefore, perturbations of the maximum conductances along singular vectors associated with large singular values will be readily observed by significant changes in the total membrane current. Conversely, a perturbation of the maximum conductances along a singular vector for which the associated singular value is zero, or very small, will not result in appreciable changes in the total membrane current and is, therefore, expected to be impossible to identify by only observing the transmembrane potential.

2. A general perturbation

Since the collection of singular vectors constitutes an orthonormal collection of vectors, any perturbed vector $\bar{\mu}$ can be written in the form

$$\bar{\mu} = \mu + \sum_{i=1}^{N} \varepsilon_i v_i$$

for appropriate choices of the constants $\{\varepsilon_i\}$. By using this representation, we find that

$$I_T - \bar{I}_T = A\mu - A\bar{\mu} = -\sum_{i=1}^{N} \varepsilon_i \sigma_i u_i,$$

so

$$\|I_T - \bar{I}_T\|^2 = \sum_{i=1}^{N} \varepsilon_i^2 \sigma_i^2 = \sum_{i=1}^{r} \varepsilon_i^2 \sigma_i^2.$$

In other words, if $\bar{\mu} - \mu$ can be expressed using only the singular vectors $\{v_i\}_{i=r+1}^N$, then $\|I_T - \bar{I}_T\|^2 = 0$, and, therefore, such a perturbation will not lead to changes in the total membrane current. On the other hand, if $\bar{\mu} - \mu$ can be expressed using the singular vectors $\{v_i\}_{i=1}^r$, then $\|I_T - \bar{I}_T\|^2 \neq 0$, and such a perturbation will lead to changes in the total membrane current.

D. The identifiability index

We have seen that, according to the SVD analysis, perturbations along vectors that can be spanned by vectors in the space $\mathcal{N}(A) = \text{span}\{v_{r+1}, \ldots, v_N\}$ cannot be identified by observing changes in the total membrane current and, conversely, that perturbations along vectors in the space $\mathcal{N}(A)^\perp = \text{span}\{v_1, \ldots, v_r\}$ can be identified. We would like to translate this result to estimate the identifiability of the unit vectors, that is, the conductances of the currents defining the AP model. In other words, we would like to characterize the identifiability of the maximum conductance of the Na-channels, the Kr-channels, and so on. Clearly, if the perturbation of the conductance vector is completely in the space $\mathcal{N}(A)$ or in the space $\mathcal{N}(A)^\perp$, the question is simple, but we need to define the identifiability of unit vectors that are partly in both spaces. We will do this by considering the projection of the perturbation to the $\mathcal{N}(A)$ space.

Let e be the unit vector corresponding to a model current. Since $\{v_1, \ldots, v_N\}$ is an orthonormal basis, we can expand any such vector e using this basis,

$$e = \sum_{i=1}^{N} (e, v_i) v_i. \tag{22}$$

Furthermore, the projection of this vector onto the space $\mathcal{N}(A) = \text{span}\{v_{r+1}, \ldots, v_N\}$ is simply given by

$$P_N e = \sum_{i=r+1}^{N} (e, v_i) v_i. \tag{23}$$

Now, e is the complete vector, $P_N e$ is the part of the vector that cannot be identified, and $e - P_N e$ is the part of the vector that

is in the space of identifiable vectors, $\mathcal{N}(A)^{\perp}$. We now define the "identifiability index" of a vector to be given by

$$k(e) = \|e - P_N e\|. \tag{24}$$

Here, it is useful to note that if $e \in \mathcal{N}(A)$, then $e = P_N e$ and $k(e) = 0$. Similarly, if $e \in \mathcal{N}(A)^{\perp}$, then $P_N e = 0$ and $k(e) = 1$ (since $\|e\| = 1$ for a unit vector). Hence, a completely unidentifiable unit vector has identifiability index equal to zero, and a completely identifiable unit vector has identifiability index equal to one.

E. Measuring the perturbation effects

In order to investigate the effect of model perturbations, we define a measure H, measuring the difference between the computed AP in the default version and a perturbed version of the model. This H is set up to detect differences in a selection of action potential characteristics and defined as

$$H(\varepsilon, v_i) = \sum_{q=1}^{5} H_q(\varepsilon, v_i), \tag{25}$$

where

$$H_1(\varepsilon, v_i) = \frac{|\mathrm{APD}_{30}(v^*) - \mathrm{APD}_{30}(\bar{v}(\varepsilon \cdot v_i))|}{|\mathrm{APD}_{30}(v^*)|}, \tag{26}$$

$$H_2(\varepsilon, v_i) = \frac{|\mathrm{APD}_{50}(v^*) - \mathrm{APD}_{50}(\bar{v}(\varepsilon \cdot v_i))|}{|\mathrm{APD}_{50}(v^*)|}, \tag{27}$$

$$H_3(\varepsilon, v_i) = \frac{|\mathrm{APD}_{80}(v^*) - \mathrm{APD}_{80}(\bar{v}(\varepsilon \cdot v_i))|}{|\mathrm{APD}_{80}(v^*)|}, \tag{28}$$

$$H_4(\varepsilon, v_i) = \frac{\left|\left(\frac{dv^*}{dt}\right)_{\max} - \left(\frac{d\bar{v}(\varepsilon \cdot v_i)}{dt}\right)_{\max}\right|}{\left|\left(\frac{dv^*}{dt}\right)_{\max}\right|}, \tag{29}$$

$$H_5(\varepsilon, v_i) = \frac{\|v^* - \bar{v}(\varepsilon \cdot v_i)\|}{\|v^*\|}. \tag{30}$$

Here, v^* is the transmembrane potential of the default model and $\bar{v}(\varepsilon \cdot v_i)$ is the transmembrane potential of a model for which the currents are perturbed by $\varepsilon \cdot v_i$, where v_i is a singular vector. Furthermore APD_{30}, APD_{50}, and APD_{80} are the action potential durations (in ms) for 30%, 50%, and 80% repolarization, respectively, $(\frac{dv}{dt})_{\max}$ is the maximal upstroke velocity (in mV/ms), and $\|\cdot\|$ is the Euclidian norm.

F. Singular values close to zero

The sensitivity index defined in Sec. II D distinguishes between singular values that are positive and those that are identically equal to zero. There is nothing wrong in defining the identifiability index in this way, but in actual computations, the main challenge is posed by singular values that are close to zero. From (21), we see that if the singular value is very small, a perturbation in the direction of the associated singular vector changes the total membrane current very little. Therefore, we would also like to include singular vectors associated with small singular values in the space of nonidentifiable vectors.

We expect that it would be difficult to select a specific threshold for the size of the singular values so that singular values below the threshold would correspond to undistinguishable perturbation effects for different AP models and simulation conditions. Therefore, we let the identifiability of a singular vector be determined by the observed changes in the APs resulting from perturbations along that singular vector. In order to formalize this, we introduce an auxiliary space S spanned by a set of singular vectors v_i

$$S = \mathrm{span}\{v_i\} \text{ for } i \text{ such that } \left\{ \max_{-0.5 \le \varepsilon \le 0.5} H(\varepsilon, v_i) < \delta \right\}. \tag{31}$$

Here, δ denotes a threshold value to be specified below, and H is defined in (25). Furthermore, the identifiability index is defined by

$$k(e) = \|e - P_S e\|, \tag{32}$$

where e is the considered perturbation vector (typically a unit vector) and $P_S e$ is the projection of e onto the auxiliary space S defined in (31).

G. Stimulation protocols and technical specifications

In all simulations presented below, a 1 ms long constant stimulus current of 40 A/F is applied every second for 20 s before recording the currents and transmembrane potential. For simulations of cells exposed to drugs (see Sec. III C), the model parameterization is changed to reflect drug effects and then paced in the same manner as above for 1000 s to define new initial conditions for the default (unperturbed) versions of the models for cells exposed to drugs. In the simulations exploring a random stimulation protocol (see Sec. III D), we apply the stimulus current at 10 randomly chosen time points during a 5000 ms long simulation (after the 20 s long stimulation protocol used in all simulations). These randomly chosen time points are given by 35.7 ms, 634.9 ms, 1392.5 ms, 2108.8 ms, 2426.9 ms, 2734.4 ms, 3161.8 ms, 3398.7 ms, 4073.6 ms and 4529.0 ms. For these simulations, we record each of the currents every time step of size $\Delta t = 0.1$ ms between $t = 0$ ms and $t = 5000$ ms in the construction of the current matrix, A [see (11)]. For the remaining simulations, we record the currents every time step of size $\Delta t = 0.1$ ms between $t = 0$ ms, and $t = 500$ ms, unless otherwise specified. All numerical simulations are conducted using the ode15s solver in Matlab.

III. RESULTS

In this section, we illustrate a few examples of the SVD analysis outlined above. We consider three AP models for human ventricular cardiomyocytes: the model of ten Tusscher *et al.*,[26] the model of Grandi *et al.*,[27] and the model of O'Hara *et al.*.[28] Note, however, that the method described here can be applied to any AP model written in the forms (5) and (6), and, thus, the method covers most commonly used models of the cardiac action potential.

We investigate the relationship between the size of the singular values and the effect of perturbing the currents by the corresponding singular vectors for these three models. In addition, we compute the identifiability index for the currents of the models. We consider both the default versions of the model and versions of the models adjusted to represent cells exposed to drugs. We also investigate how the SVD analysis is affected by the size of the time step, Δt, used to record the currents and transmembrane potential, and how the identifiability of the currents is affected when a random stimulation protocol is applied.

A. Singular value decomposition of the currents in the ten Tusscher, Grandi, and O'Hara AP models

Figures 1, 2, and 3 show the SVD analysis of the currents in the ten Tusscher model,[26] the Grandi model,[27] and the O'Hara model,[28] respectively. We consider the epicardial version of all the AP models.

In the Grandi model, a number of currents (I_{Na}, I_{bNa}, I_{NaK}, I_{Ks}, I_{pK}, I_{ClCa}, I_{CaL}, I_{NaCa}, I_{pCa}, and I_{bCa}) are divided into two components, one directed into the junctional cleft and one directed into the subsarcolemmal space. In the analysis below, the currents of each type represent the sum of these two components. Furthermore, both in the Grandi model and in the O'Hara model, the L-type calcium current is divided into three ionic components; a calcium component, a sodium component., and a potassium component. In the analysis below, the current I_{CaL} is defined as the sum of these three components.

1. Singular values and vectors

Figure 1 shows the 12 singular values $\sigma_1, \ldots, \sigma_{12}$, of the SVD of the 12 currents in the ten Tusscher model, ordered from the largest value, $\sigma_1 = 420.26$, to the smallest value, $\sigma_{12} = 0.0063$. The plots located directly below each singular value illustrate the corresponding singular vectors. Each letter between "a" and "l" here corresponds to a specific current in the ten Tusscher model, specified in the orange panel on the right-hand side. The intensity of the green background color of the plots corresponds to the size of the singular value.

We observe that the largest singular value, σ_1, corresponds to a singular vector that is almost equal to the unit vector e_{Na} for the fast sodium current. In addition, the smallest singular value, σ_{12}, corresponds to a singular vector quite close to the unit vector e_{bNa} for the background sodium current, but also with a small contribution from the background calcium current, I_{bCa}.

The Grandi model and the O'Hara model consist of 15 and 13 membrane currents, respectively, and Figs. 2 and 3 similarly show the singular values and corresponding singular vectors for these two models. We observe that for all the three models, the largest singular value corresponds to a singular vector almost exclusively associated with the fast sodium current, I_{Na}. In addition, we observe that the size of the singular values varies between small values in the range 0.0001–0.01 to large values of about 300–400 for each of the three considered AP models.

2. Connection between the singular values and the effect of perturbations

According to the SVD analysis outlined above, perturbations of the model currents corresponding to large singular values are expected to result in large effects on the total membrane current, I_T, and thereby, expectedly, to large effects on the resulting action potential. Conversely, perturbations corresponding to small singular values are expected to result in small effects on the total membrane current and the resulting action potential. This theoretical result relies on simplifying assumptions, and, consequently, it might not hold in actual AP model computations. We, therefore, wish to investigate whether the expected results about the connection between the size of the singular values and the effect of the perturbation hold for the three AP models considered in Figs. 1–3.

To investigate this, we run simulations in which each of the model currents are perturbed by the computed singular vectors. More specifically, for each singular vector v_i, each of the currents I_j of the model is multiplied by the factor $(1 + \varepsilon \cdot v_{i,j})$, where $v_{i,j}$ denotes the jth element of the singular vector v_i, and ε is varied between -0.5 and 0.5. For example, in the case of the first singular value, σ_1, of the ten Tusscher model (see Fig. 1), the fast sodium current, I_{Na}, is multiplied by a factor close to $(1 + \varepsilon)$, while the other currents are almost unperturbed. For the second singular value, σ_2, I_{to} is multiplied by a factor of approximately $(1 + 0.5 \cdot \varepsilon)$, I_{CaL} is multiplied by approximately $(1 - 0.8 \cdot \varepsilon)$, and the remaining currents are only perturbed by very small factors.

In each of Figs. 1–3, the left plots below the singular vector plots show the measure, H, defined in (25) measuring the difference between the computed AP in the default version of the models and the perturbed models for each of the singular values. The text in the upper part of the plots indicates the maximum value of $H(\varepsilon, v_i)$ computed for the considered values of ε, ignoring cases where any of the action potential features of H_1–H_5 are not possible to compute. Furthermore, the right plots illustrate the computed action potentials for a small selection of ε-values ($\varepsilon = -0.5, -0.2, 0, 0.2, 0.5$).

In the plots, we observe that, in general, the expected observation that perturbations corresponding to large singular values will result in large changes in the AP and that perturbations corresponding to small singular values will result in small changes in the AP seems to hold well for each of the three considered AP models. We observe that the effect of a perturbation corresponding to a given singular value is not necessarily larger than the effect of a perturbation corresponding to a smaller singular value in all cases, but the largest perturbation effects are observed for the largest singular values, and the small singular values seem to result in quite small perturbation effects in most cases.

For the ten Tusscher model, we observe that perturbations corresponding to the singular values σ_4 and $\sigma_6, \ldots, \sigma_{12}$ all result in relatively small changes in the computed AP, with values of H below 0.25. Similarly, for the Grandi model, perturbations corresponding to $\sigma_7, \ldots, \sigma_{15}$, result in very small changes of the computed AP. For the O'Hara model, perturbations corresponding to the singular values $\sigma_4, \ldots, \sigma_{13}$ all result in nearly indistinguishable changes in the computed AP.

3. Identifiability index for individual currents

As observed in Figs. 1–3, perturbations corresponding to large singular values seem to result in large effects of the computed AP, whereas perturbations corresponding to small singular values result in relatively small effects on the computed AP. As indicated in Sec. II, we wish to use this knowledge to construct an identifiability index that describes the identifiability of a single current.

The identifiability index defined in (32) computed for each of the currents in Figs. 1–3 for $\delta = 0.25$ are shown in the orange panel on the right-hand side of the figures. For the ten Tusscher model, the I_{Na}, I_{to}, I_{CaL}, and I_{Ks} currents obtain relatively high values of the identifiability index (above 0.83), while the currents I_{bNa}, I_{pCa}, I_{bCa}, I_{K1}, I_{NaCa}, I_{Kr}, and I_{NaK} obtain quite small values (below 0.32). For the Grandi model, the identifiability index is high (above 0.88) for I_{Na}, $I_{to,f}$, I_{CaL}, I_{bCl}, I_{K1}, and I_{NaCa}, and the identifiability index is low

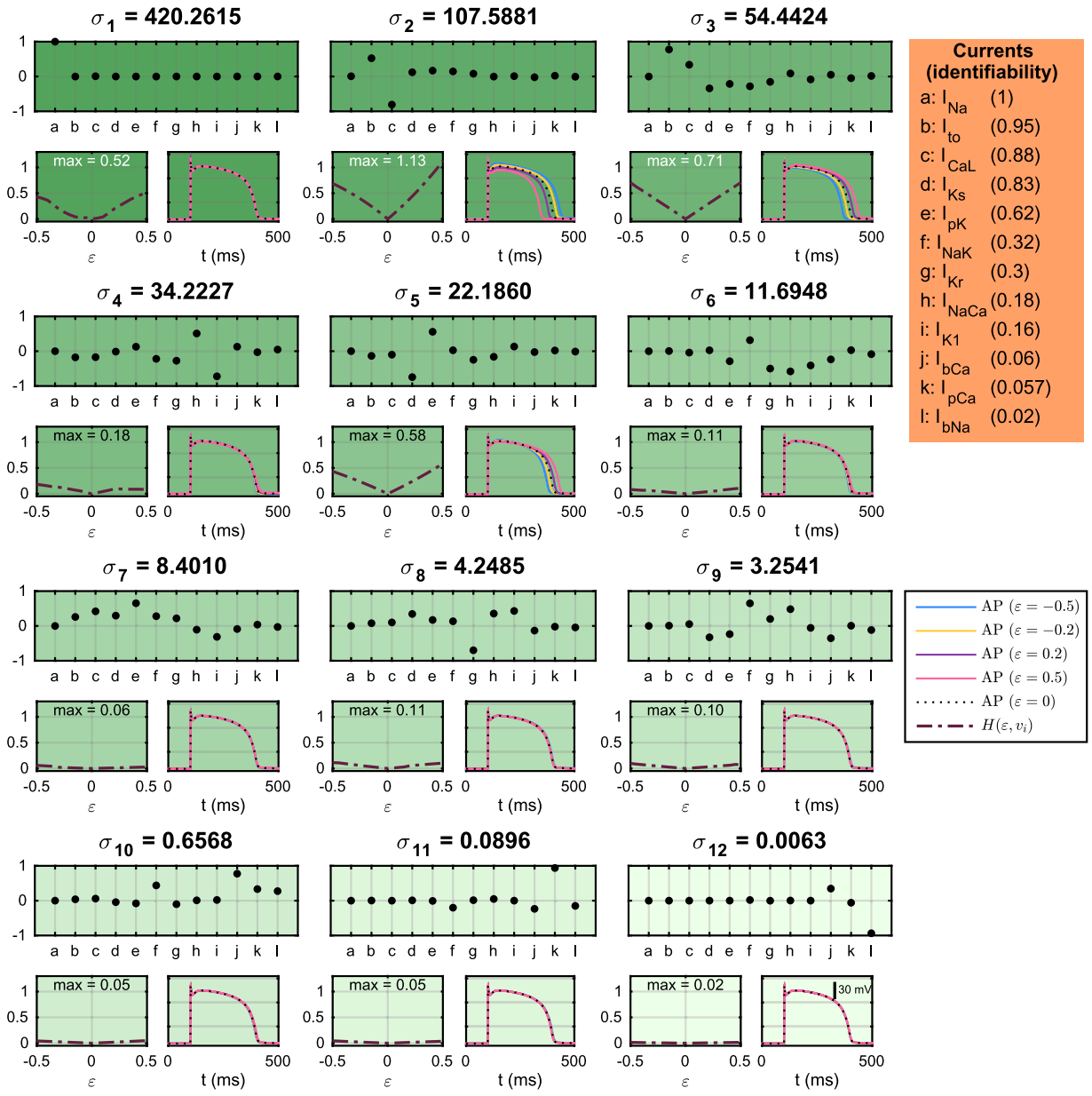

FIG. 1. SVD analysis of the currents of the ten Tusscher model.[26] The values $\sigma_1, \ldots, \sigma_{12}$ are the singular values of the current matrix A defined in (11). The plots directly below the singular values are the singular vectors corresponding to each of the singular values. Each letter corresponds to a single current specified in the orange panel to the right. The below plots show how a perturbation of the currents corresponding to the singular vector affects the computed AP of the model. The left plots show the measure $H(\varepsilon, v_i)$, defined by (25). The right plots show the computed action potentials for a selection of perturbations. The numbers given after each current in the orange right panel indicate the identifiability index (32) computed for each of the currents. The auxiliary space S is defined by (31) with $\delta = 0.25$.

(below 0.42) for the remaining currents. Similarly, I_{Na} and I_{Kr} have high values of the identifiability index (above 0.91) in the O'Hara model, whereas I_{NaK}, I_{NaCa}, I_{K1}, I_{bK}, I_{NaL}, I_{Ks}, I_{bNa}, I_{bCa}, and I_{pCa} have small values of the identifiability index (below 0.2).

B. Effect of the size of the time step Δt

In the SVD analysis reported in Figs. 1–3, we record the currents and transmembrane potential in every time step of size $\Delta t = 0.1$ ms. In order to investigate the effect of the time step on the analysis, we

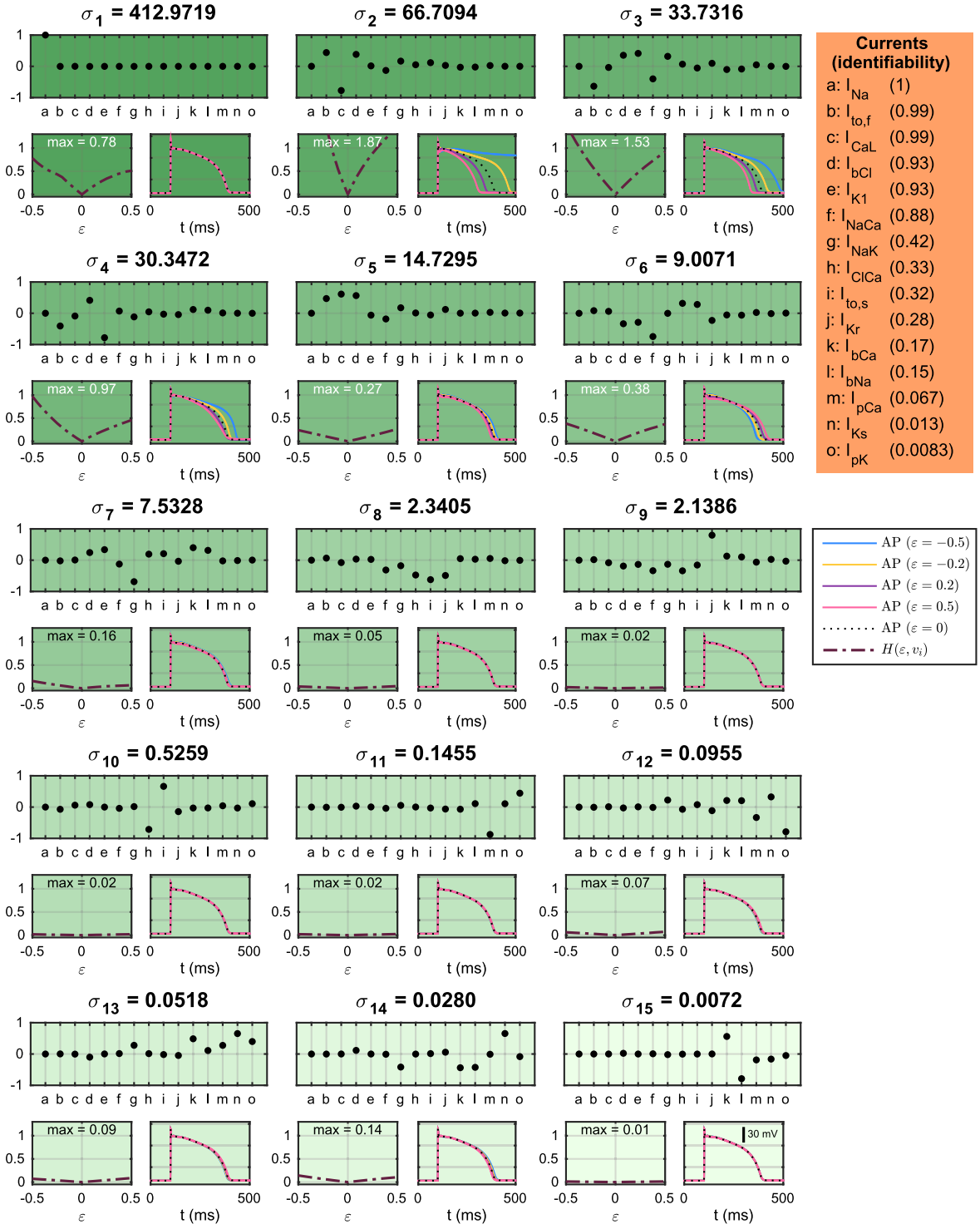

FIG. 2. SVD analysis of the currents of the Grandi model,[27] following the same structure as Fig. 1.

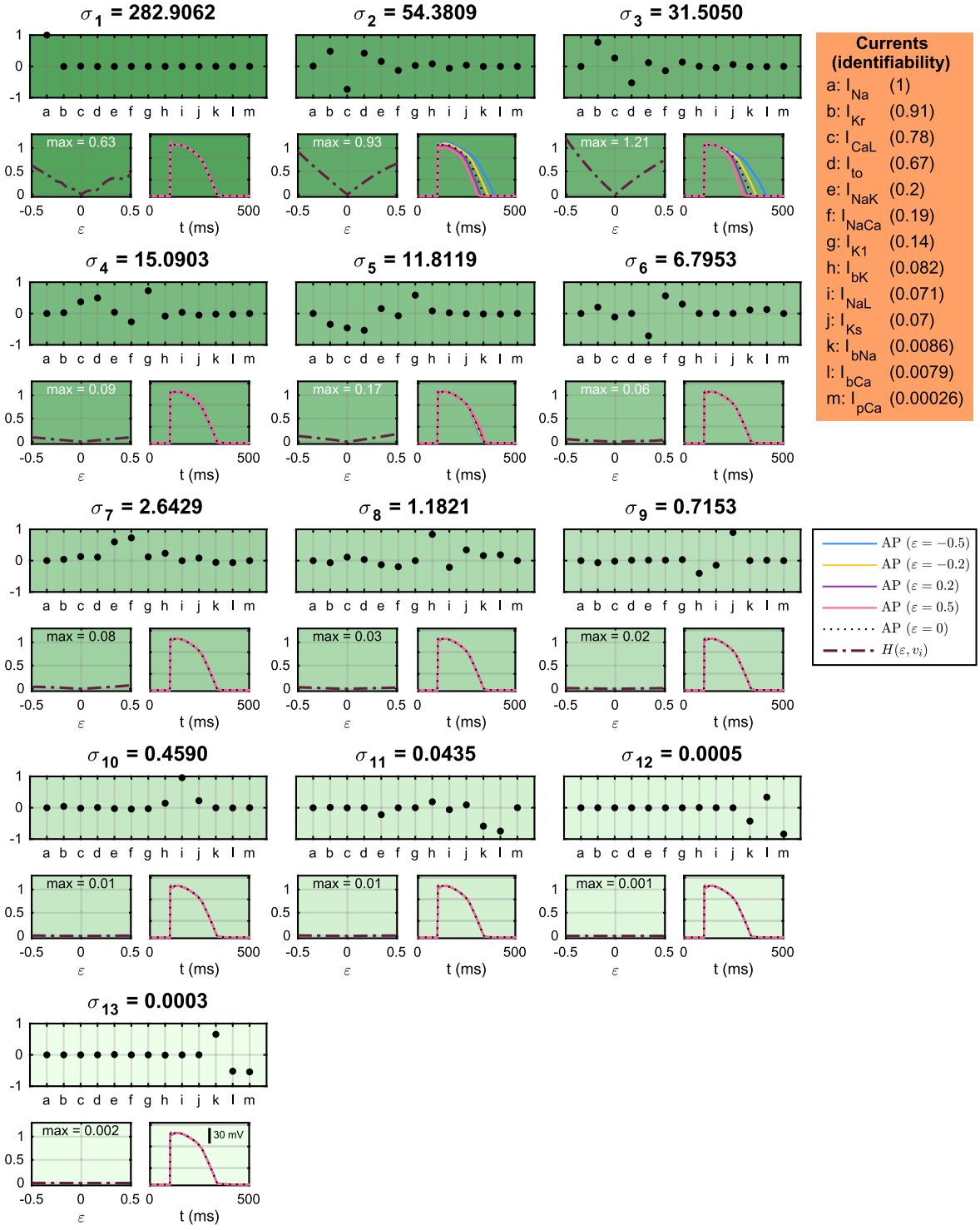

FIG. 3. SVD analysis of the currents of the O'Hara model,[28] following the same structure as Fig. 1.

TABLE I. Results from SVD analysis using the ten Tusscher model and four different time steps Δt for recording the currents and transmembrane potential. The upper rows report the largest and smallest singular values, and the lower rows report the computed identifiability indices defined by (32) and (31).

Δt (ms)	0.01	0.1	1	2
σ_1	1309.9	420.3	138.1	24.7
σ_{12}	0.02	0.0063	0.0018	0.0012
σ_{12}/σ_1	1.5×10^{-05}	1.5×10^{-05}	1.3×10^{-05}	4.9×10^{-05}
Identifiability index				
I_{Na}	1.00	1.00	0.002	0.002
I_{to}	0.95	0.95	0.95	0.95
I_{CaL}	0.88	0.88	0.88	0.88
I_{Ks}	0.83	0.83	0.83	0.83
I_{pK}	0.62	0.62	0.62	0.61
I_{NaK}	0.32	0.32	0.32	0.31
I_{Kr}	0.30	0.30	0.30	0.30
I_{NaCa}	0.18	0.18	0.19	0.19
I_{K1}	0.16	0.16	0.15	0.15
I_{bCa}	0.06	0.06	0.06	0.06
I_{pCa}	0.06	0.06	0.06	0.06
I_{bNa}	0.02	0.02	0.02	0.02

TABLE II. Results from SVD analysis using the Grandi model and four different values of the time step Δt for recording the currents and transmembrane potential. The upper rows report the largest and smallest singular values, and the lower rows report the computed identifiability indices defined by (32) and (31).

Δt (ms)	0.01	0.1	1	2
σ_1	1333.8	413.0	330.3	15.0
σ_{15}	0.023	0.0072	0.0018	0.00021
σ_{15}/σ_1	1.7×10^{-05}	1.7×10^{-05}	5.3×10^{-06}	1.4×10^{-05}
Identifiability index				
I_{Na}	1.00	1.00	1.00	0.97
$I_{to,f}$	0.99	0.99	0.99	0.99
I_{CaL}	0.99	0.99	0.99	0.99
I_{bCl}	0.93	0.93	0.93	0.93
I_{K1}	0.93	0.93	0.93	0.93
I_{NaCa}	0.88	0.88	0.88	0.87
I_{NaK}	0.42	0.42	0.42	0.42
I_{ClCa}	0.33	0.33	0.34	0.34
$I_{to,s}$	0.32	0.32	0.32	0.32
I_{Kr}	0.28	0.28	0.29	0.29
I_{bCa}	0.17	0.17	0.17	0.18
I_{bNa}	0.15	0.15	0.14	0.15
I_{pCa}	0.07	0.07	0.07	0.07
I_{Ks}	0.01	0.01	0.01	0.02
I_{pK}	0.01	0.01	0.01	0.22

report in Tables I–III results from similar experiments where the currents and transmembrane potential are recorded for time steps of size $\Delta t = 0.01$ ms, 0.1 ms, 1 ms, and 2 ms. The upper rows of the tables report the maximum and minimum singular values of the current matrix A, as well as the ratio between the smallest and largest singular values. The next rows show the identifiability indices computed in each case for each of the currents.

We observe that as the time step used to record the currents is decreased, the largest and smallest singular values both seem to increase, but the ratio between the smallest and largest singular values remain roughly of the same size. In fact, for small values of Δt, both the smallest and the largest singular values seem to be proportional to $\Delta t^{-1/2}$. Furthermore, we observe that in most cases, the identifiability indices are very similar for the different values of Δt. An exception is observed for the time step of 1 ms or 2 ms for the ten Tusscher model. In that case, the analysis predicts that I_{Na} is largely unidentifiable even though the current is characterized as highly identifiable for smaller values of Δt. This suggests that a Δt of 1 ms might be too large to accurately characterize the identifiability of the currents. Indeed, the fast sodium current, I_{Na}, is almost only active during the upstroke of the action potential, and in Fig. 7, we see that the upstroke of the action potential in the ten Tusscher model lasts for less than 2 ms. Therefore, it is not surprising that a time step of less than 1 ms is probably required to capture the relevant information about I_{Na}. However, the time step of $\Delta t = 0.1$ ms appears to be sufficient and will be used in the remaining computations.

C. Identifiability in the presence of drugs

Figures 1–3 show the SVD analysis and identifiability indices computed for the default versions of the ten Tussscher, Grandi, and O'Hara AP models. In order to investigate how the identifiability of the individual model currents changes under different conditions, Tables IV–VI compare the identifiability indices computed for the default models to those computed for models adjusted to represent exposure to two drugs, Verapamil and Cisapride. The presence of the drugs are modeled as in Ref. 19, i.e., by reducing the maximum conductance of I_{CaL} by 50% and the maximum conductance of I_{Kr} by 25% for Verapamil and reducing the maximum conductance of I_{Kr} by 50% for Cisapride.

In Tables IV–VI, we observe that the identifiability indices vary a bit between the three versions of the models for some of the currents, but for each of the models, the currents with identifiability index close to one and the currents with identifiability index close to zero seem to be quite consistent for both the control case and under the simulated effects of the two drugs. Some of the considerable changes in identifiability is observed for the I_{NaCa} and I_{NaK} currents in the Grandi model. For I_{NaCa}, the identifiability drops from 0.88 in the no drug case to 0.43 in the presence of Verapamil. For I_{NaK}, the identifiability increases from 0.42 to 0.81 in the presence of Cisapride. In addition, the identifiability index of I_{K1} increases from 0.14 in the no drug case to 0.98 in the presence of Verapamil in the O'Hara model.

D. Identifiability for a random stimulation protocol

In Ref. 15, approaches for improving the identifiability of the maximum conductances of AP models were investigated. One of the suggested approaches for increasing the identifiability of currents that were largely unidentifiable from a single paced action potential was to apply a random stimulation protocol in which the stimulation current was applied at a number of randomly chosen points in time.

TABLE III. Results from SVD analysis using the O'Hara model and four different values of the time step Δt for recording the currents and transmembrane potential. The upper rows report the largest and smallest singular values, and the lower rows report the computed identifiability indices defined by (32) and (31).

Δt (ms)	0.01	0.1	1	2
σ_1	894.5	282.9	88.9	88.7
σ_{13}	0.00098	0.00031	8.7×10^{-05}	1.9×10^{-05}
σ_{13}/σ_1	1.1×10^{-06}	1.1×10^{-06}	9.8×10^{-07}	2.1×10^{-07}
Identifiability index				
I_{Na}	1.00	1.00	1.00	1.00
I_{Kr}	0.91	0.91	0.91	0.91
I_{CaL}	0.78	0.78	0.78	0.77
I_{to}	0.67	0.67	0.68	0.68
I_{NaK}	0.20	0.20	0.20	0.20
I_{NaCa}	0.19	0.19	0.19	0.19
I_{K1}	0.14	0.14	0.14	0.14
I_{bK}	0.08	0.08	0.08	0.08
I_{NaL}	0.07	0.07	0.07	0.07
I_{Ks}	0.07	0.07	0.07	0.07
I_{bNa}	0.01	0.01	0.01	0.01
I_{bCa}	0.01	0.01	0.01	0.01
I_{pCa}	0.0003	0.0003	0.0003	0.0003

In Ref. 15, it was found that this method improved the parameter identifiability for some of the model conductances.

In Figs. 4–6, we apply the above described SVD analysis to investigate a similar approach for the ten Tusscher, Grandi, and O'Hara models. We apply a stimulus current at ten randomly chosen points in time during a 5000 ms simulation (see Sec. II G for the specific stimulation times). The figures follow the same structure as Figs. 1–3 except that an extra row of plots is added for each singular value. This row shows the computed transmembrane potential resulting from a selection of perturbations along the singular vectors for the entire 5000 ms simulation. The center right plots show the corresponding solutions for a small time sample. In the computation of H (center left plots), we compute the value of each of the terms H_1–H_5 defined in (26)–(30) for each of the ten computed action potentials

TABLE IV. The identifiability index defined by (32) and (31) with $\delta = 0.25$ computed for the default version of the ten Tusscher model (as in Fig. 1) and for the ten Tusscher model adjusted to represent cells exposed to two drugs, Verapamil and Cisapride. Verapamil is modeled by reducing the maximum conductance of I_{CaL} and I_{Kr} by 50% and 25%, respectively. Cisapride is modeled by reducing the maximum conductance of I_{Kr} by 50%.

	No drug	Verapamil $0.5 \cdot g_{CaL}$, $0.75 \cdot g_{Kr}$	Cisapride $0.5 \cdot g_{Kr}$
Identifiability index			
I_{Na}	1.00	1.00	1.00
I_{to}	0.95	0.98	0.95
I_{CaL}	0.88	0.92	0.88
I_{Ks}	0.83	0.85	0.87
I_{pK}	0.62	0.21	0.64
I_{NaK}	0.32	0.35	0.32
I_{Kr}	0.30	0.43	0.14
I_{NaCa}	0.18	0.16	0.14
I_{K1}	0.16	0.28	0.15
I_{bCa}	0.06	0.10	0.05
I_{pCa}	0.06	0.04	0.06
I_{bNa}	0.02	0.03	0.02

TABLE V. The identifiability index defined by (32) and (31) with $\delta = 0.25$ computed for the default version of the Grandi model (as in Fig. 2) and for the Grandi model adjusted to represent cells exposed to the two drugs, Verapamil and Cisapride.

	No drug	Verapamil $0.5 \cdot g_{CaL}$, $0.75 \cdot g_{Kr}$	Cisapride $0.5 \cdot g_{Kr}$
Identifiability index			
I_{Na}	1.00	1.00	1.00
$I_{to,f}$	0.99	0.99	0.99
I_{CaL}	0.99	0.99	0.99
I_{bCl}	0.93	0.90	0.98
I_{K1}	0.93	0.89	1.00
I_{NaCa}	0.88	0.43	0.89
I_{NaK}	0.42	0.39	0.81
I_{ClCa}	0.33	0.05	0.39
$I_{to,s}$	0.32	0.17	0.37
I_{Kr}	0.28	0.11	0.14
I_{bCa}	0.17	0.17	0.44
I_{bNa}	0.15	0.14	0.35
I_{pCa}	0.07	0.06	0.07
I_{Ks}	0.01	0.006	0.02
I_{pK}	0.01	0.005	0.01

TABLE VI. The identifiability index defined by (32) and (31) with $\delta = 0.25$ computed for the default version of the O'Hara model (as in Fig. 3) and for the O'Hara model adjusted to represent cells exposed to the two drugs, Verapamil and Cisapride.

	No drug	Verapamil $0.5 \cdot g_{CaL}$, $0.75 \cdot g_{Kr}$	Cisapride $0.5 \cdot g_{Kr}$
Identifiability index			
I_{Na}	1.00	1.00	1.00
I_{Kr}	0.91	0.97	0.90
I_{CaL}	0.78	0.97	0.92
I_{to}	0.67	1.00	0.90
I_{NaK}	0.20	0.26	0.32
I_{NaCa}	0.19	0.22	0.27
I_{K1}	0.14	0.98	0.54
I_{bK}	0.08	0.17	0.15
I_{NaL}	0.07	0.12	0.10
I_{Ks}	0.07	0.10	0.20
I_{bNa}	0.01	0.02	0.01
I_{bCa}	0.01	0.02	0.01
I_{pCa}	0.0003	0.0003	0.0004

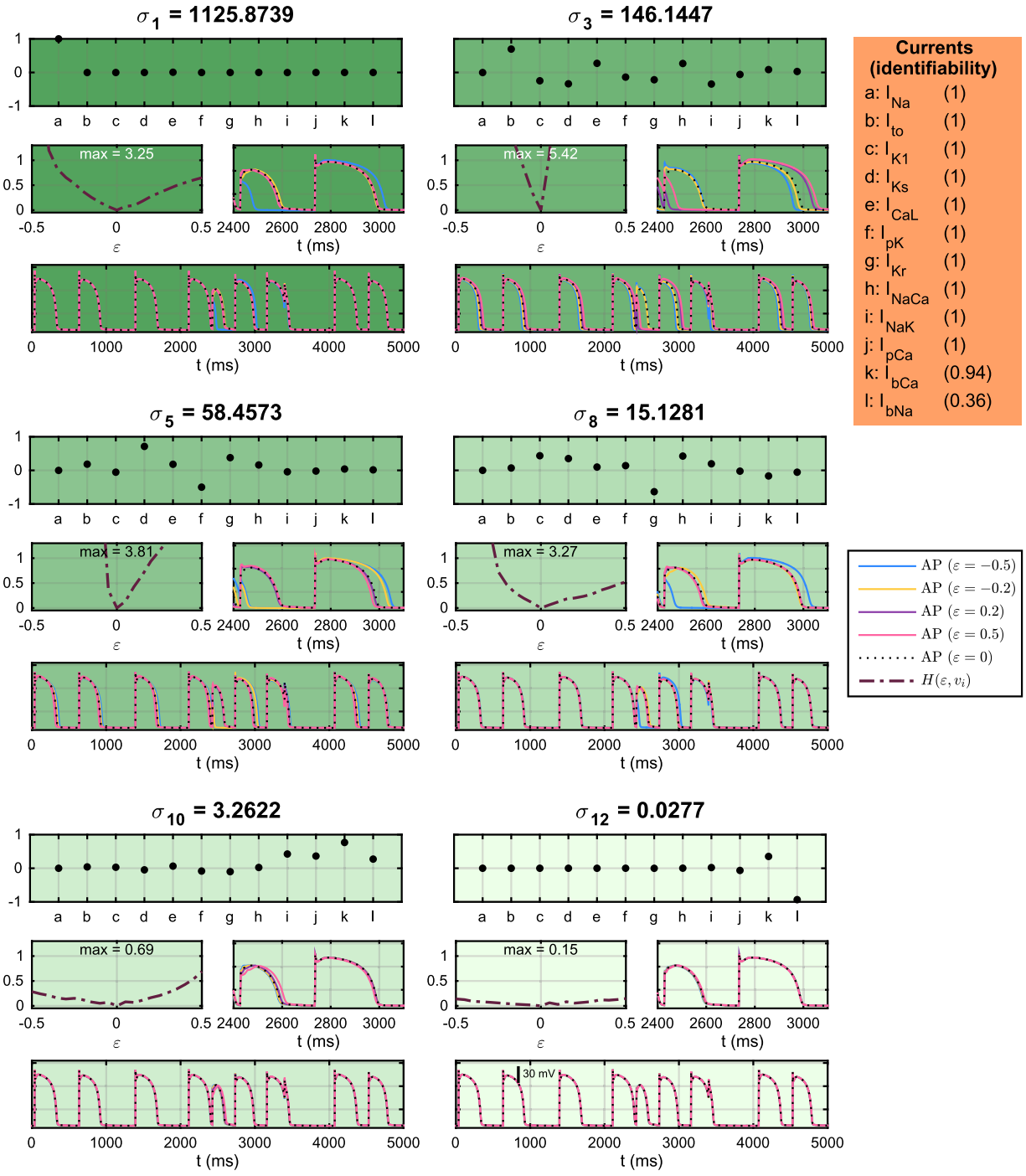

FIG. 4. SVD analysis of the currents of the ten Tusscher model[26] using a random stimulation protocol with a stimulation current applied at ten randomly chosen points in time during a 5000 ms period. The values σ_1, σ_3, σ_5, σ_8, σ_{10}, and σ_{12} are a selection of the singular values of the current matrix, A, defined in (11). The plots directly below the singular values show the corresponding singular vectors. The center left plots show the measure $H(\varepsilon, v_i)$, defined by (25). The center right plots show the computed action potentials for a selection of perturbations for a small time interval. The lower plots show the corresponding solutions for the entire 5000 ms period. The numbers given after each current in the orange right panel indicate the identifiability index defined by (32) and (31) with $\delta = 0.25$.

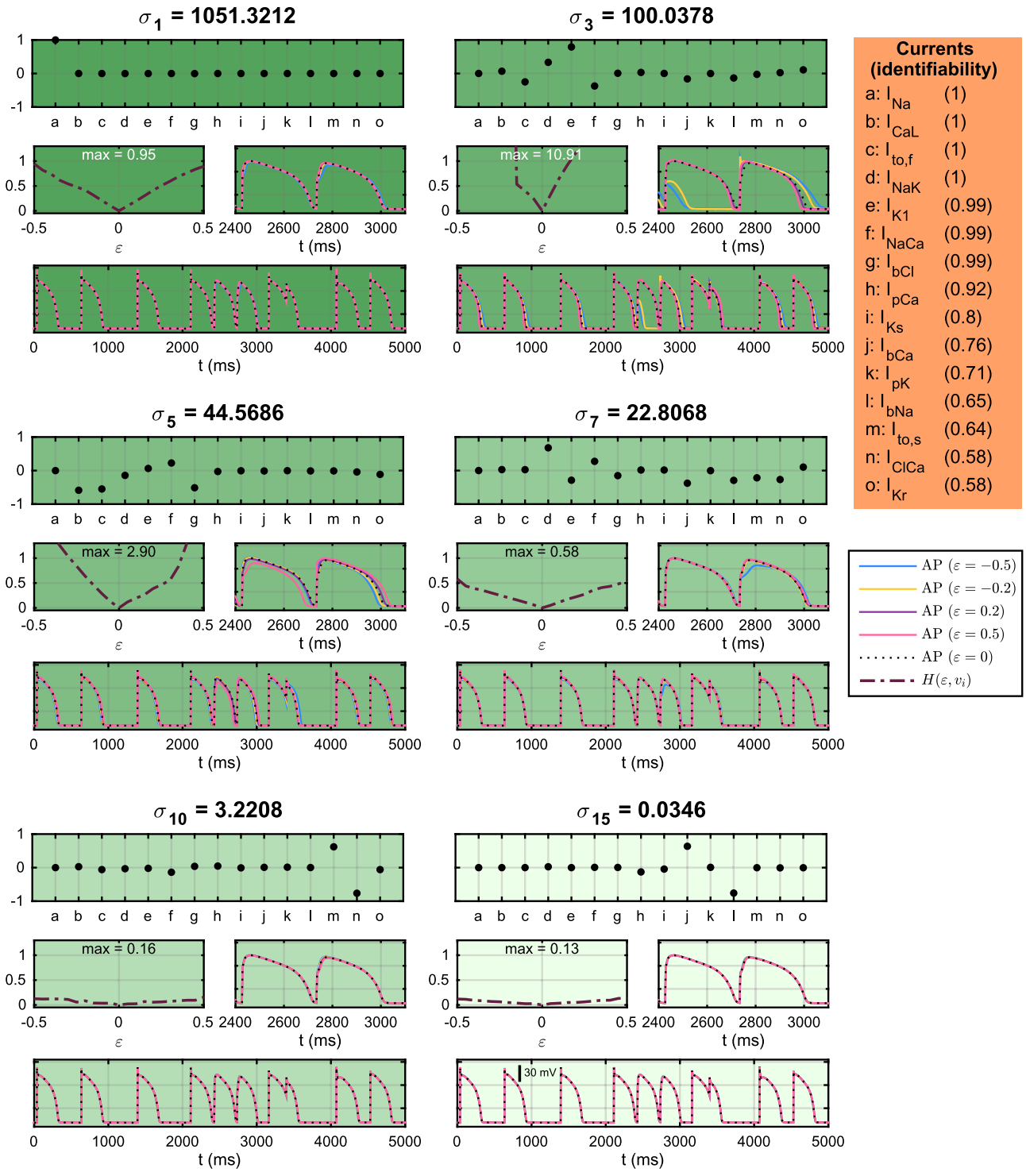

FIG. 5. SVD analysis of the currents of the Grandi model[27] using a random stimulation protocol. The figure follows the same structure as Fig. 4.

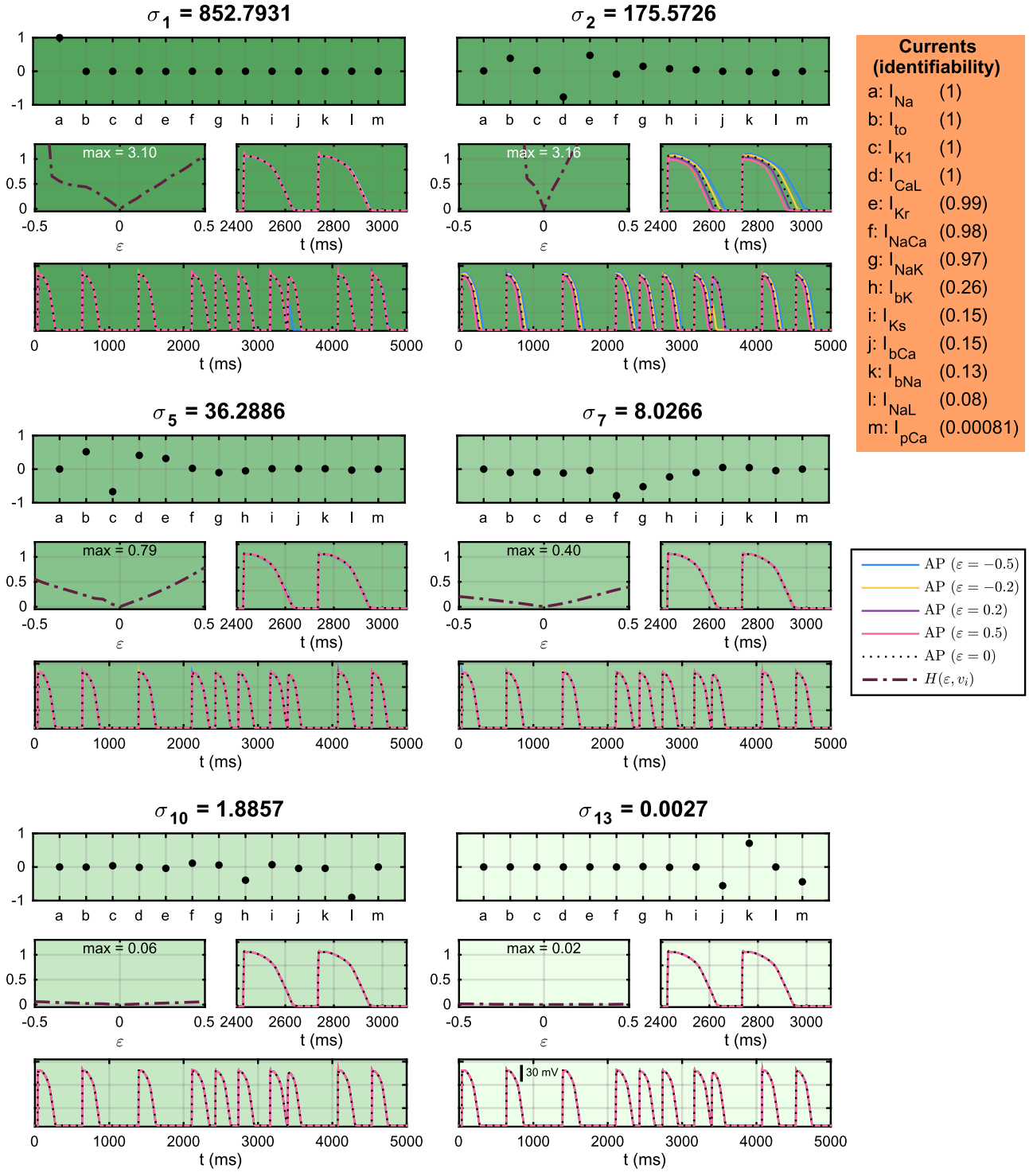

FIG. 6. SVD analysis of the currents of the O'Hara model[28] using a random stimulation protocol. The figure follows the same structure as Fig. 4.

(i.e., from the solution between each stimulation). In the computation of the final H defined in (25), we include the maximum value of each $H_j, j = 1, \ldots, 5$ over the ten computed action potentials. Furthermore, for reasons of space, we only show the singular vectors and perturbation effects for a selection of six singular values in Figs. 4–6.

In the table reporting the identifiability index in Fig. 4, we observe that the random pacing protocol greatly increases the identifiability of a number of currents in the ten Tusscher model. For example, the identifiability of I_{pCa}, I_{K1}, I_{NaCa}, I_{Kr}, and I_{NaK} is increased from 0.057, 0.16, 0.18, 0.3, and 0.32, respectively, for the default stimulation protocol in Fig. 1 to a value of 1 in the random stimulation protocol in Fig. 4. For the random stimulation protocol only a single current, I_{bNa}, obtains an identifiability of less than 0.9. In Figs. 5 and 6, we similarly observe that the random stimulation protocol increases the identifiability of a number of currents in the Grandi and O'Hara models.

IV. DISCUSSION

It is important to understand the uncertainty of the parameters in AP models. An overview of related problems involved in AP models of cardiac cells is given by Johnstone *et al.*[29] One of the problems highlighted in the paper is that there are unidentifiable parameters in the AP model—"multiple parameter sets fit the data equally well and the individual conductances cannot be identified. . .." Here, we have developed a method for investigating the identifiability of the maximum conductances of ion channels in a model, when the model is parameterized to fit a single action potential waveform. Simulations of the AP model give the total transmembrane currents and the individual ion currents. Then, by storing the currents in a matrix, the SVD method can be used to analyze what combinations of currents will be largely invisible in the overall waveform. We have developed an identifiability index that uses this information to quantify how identifiable the individual currents are. Although the method is based on linear analysis of a highly nonlinear problem, the method gives valuable insight that is difficult to obtain by other methods.

A. Perturbation effects

In Figs. 1–3, we observed that large singular values were associated with large perturbation effects along their corresponding singular vectors, while small singular values were to a large degree associated with small perturbation effects, as predicted by the linear theoretical considerations outlined in Sec. II. In all three figures, the nonlinear perturbation effects were considered by the use of a measure H defined in (25) (lower left plots) to detect differences in the perturbed AP waveform, and in many cases, the trends of H could be readily seen by simply visually inspecting the APs resulting from the perturbations (lower right plots).

In some cases, however, the perturbations produced large values of H even though the perturbed APs seemed to be visually identical. The reason why in these cases H measures large differences is that H includes a term that measures the effect on the maximal upstroke velocity. This effect is hard to observe in the plots of the AP due to the time scale, but the effect is illustrated for two examples from the ten Tusscher model in the lower panel of Fig. 7. Here, we show the upstroke of the AP for perturbations along the singular vectors corresponding to the largest singular value (left) and the smallest singular value (right) of the SVD analysis. For the large singular value, σ_1, we observe large changes in the upstroke dynamics, which correspond to the large values of H observed in Fig. 1. For the smallest singular value, σ_{12}, on the other hand, the effects of the perturbations on the upstroke are completely indistinguishable, corresponding to the small values of H observed in Fig. 1.

B. The identifiability index

In order to deduce information about the identifiability of the maximum conductance of the individual model currents from

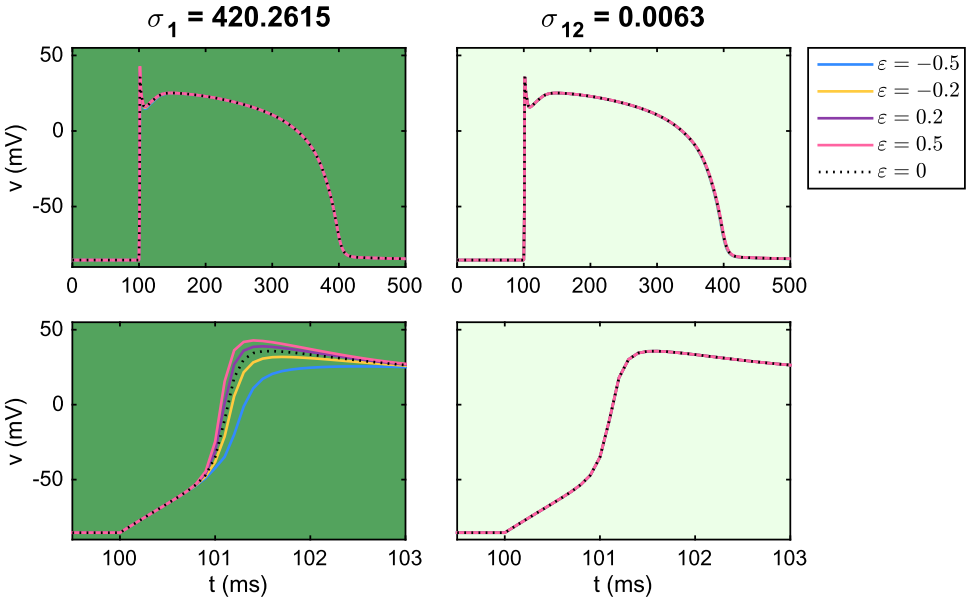

FIG. 7. Effect on the transmembrane potential of perturbing the currents corresponding to the largest singular value, σ_1, and the smallest singular value, σ_{12}, of the SVD analysis of the ten Tusscher model (see Fig. 1). The upper panel shows the full action potential, and the lower panel focuses only on the upstroke.

the information gained from the SVD analysis, we defined an identifiability index given by (32), measuring the difference between the unit vector of the current and the projection of the unit vector to the unidentifiable space defined in Sec. II F. If the identifiability index is close to zero, the current lies almost entirely in the unidentifiable space, and is expected to be hard to identify. Similarly, if the identifiability index is close to one, the current lies almost entirely in the identifiable space, and we expect that the maximum conductance of the current is easier to identify. In Figs. 1–3, we observed that this index characterized a few model currents in the ten Tusscher, Grandi, and O'Hara models as highly identifiable, while other currents were identified as largely unidentifiable. A weakness with this index is that we need to introduce a parameter δ in order to define the subspace of unidentifiable vectors; see (31). In our computations, this parameter has been set to 0.25, but in general the parameter needs to be determined using numerical experiments with the model under consideration.

1. Effect of the time step

In Tables I–III, we investigated the effect of the time step, Δt, used to record the current matrix, A. We observed that the size of the singular values of A changed when different time steps were used. Moreover, for small values of Δt, the size of the singular values seemed to be proportional to $\Delta t^{-1/2}$. However, the identifiability of the individual model currents remained relatively constant for the different time steps. Yet for the ten Tusscher model, the identifiability index of the I_{Na} current dropped from 1 for $\Delta t = 0.01$ ms or $\Delta t = 0.1$ ms to 0.002 for $\Delta t = 1$ ms or $\Delta t = 2$ ms, which suggests that a time step of less than 1 ms is probably needed to accurately capture the relevant information about the currents and, in particular, the fast sodium current, I_{Na}. The difficulties related to identifying the sodium current using relatively long time steps is commensurate with the problems encountered in Ref. 19, where coarse time resolution rendered the sodium current unidentifiable using voltage sensitive dyes.

2. Effect of the simulation conditions

In Tables IV–VI, we investigated the identifiability of the currents in models adjusted to represent cells exposed to two drugs. We observed that the identifiability of certain currents was clearly affected by the change in conditions, but that the currents characterized as highly identifiable and the ones characterized as largely unidentifiable remained relatively unchanged under the different conditions.

In Figs. 4–6, we similarly investigated how the identifiability was affected when a random stimulation protocol was applied. In Ref. 15, this approach was shown to increase the identifiability of the maximum conductance of currents in AP models. Consistent with the results in Ref. 15, the SVD analysis suggested that the identifiability of a number of model currents in the ten Tusscher, Grandi, and O'Hara AP models would increase using such a random stimulation protocol.

C. Uniqueness of model parameters

A key question in deriving and applying AP models is the uniqueness of the parameters. For Markov models used to represent the open probability of ion channels, this problem was carefully studied by Fink and Noble[30] who found parameter unidentifiability in 9 out of 13 models. Lack of uniqueness has also been observed for models of the AP of neurons (see, e.g., Refs. 31–33) and for AP models of cardiomyocytes (see, e.g., Refs. 34–37). The most common way of investigating the sensitivity of AP models is to perturb individual currents and look for the effect. This method is useful in the sense that it indicates how well blocking of individual currents can be identified using the model. Suppose, for instance, that the AP model is very sensitive to changes in the sodium current. Then, if a sodium blocker is applied, such changes will be observed, and, thus, the effect of a sodium blocker can be identified. But this approach will not uncover the identifiability of more subtle effects where a blocker affects many currents simultaneously.

The numerical examples presented above show that very few ion currents can be completely identified by observing the total membrane currents. According to the identifiability index, less than 50% of the perturbations can be observed for 7 out of 12 ion currents in the ten Tusscher model, 9 out of 15 ion currents in the model of Grandi *et al.*, and 9 out of 13 ion currents in the O'Hara model using the default stimulation protocol in Figs. 1–3. This indicates a considerable degree of redundancy in the models in their ability to produce a single paced action potential. However, for the random stimulation protocol in Figs. 4–6, the identifiability index was smaller than 0.5 only for 1 of the currents in the ten Tusscher model, 0 of the currents in the Grandi model, and 6 of the currents in the O'Hara model.

D. Model reduction

Several authors have used redundancy of AP models to derive reduced models. For instance, in both Refs. 38 and 39, the authors used redundancy of the AP models to systematically reduce complex models to obtain simpler models. Other authors have developed parsimonious models by only including major currents; see, e.g., Refs. 40–44. A comprehensive overview of models of the cardiac AP is given in Ref. 9, where models ranging from 2 to 67 variables are presented. Model reduction can be achieved by identifying insensitive parameters using the SVD method, and, more generally, this problem is often addressed by the method of proper orthogonal decomposition (POD); see, e.g., Refs. 45 and 46.

E. Linear sensitivity analysis

Over the past decade, a series of papers by Sobie and coauthors (see Refs. 47–50) have developed a theory describing a strong correlation between model parameters like the maximum conductances of the ion channels and output variables like the APD. These relations are surprising given the strong nonlinearities involved in the AP models, but the relations are also very useful, in particular, in order to understand the behavior of populations of models. We have used the fact that linear models seem to pick up important features of nonlinear AP models to devise a method for analyzing how the total transmembrane current changes under perturbations of the individual ion currents using the SVD algorithm.

V. CONCLUSION

We have presented a method for investigating the uniqueness of parameters of commonly used mathematical models of action potentials. The method is simple to implement and the results are interpreted in a straightforward manner. For three well-known models of human cardiac cells, the method revealed that significant changes in the maximum conductances can be introduced without any appreciable change in the resulting action potential. The method uses the singular value decomposition to find perturbations that give minimal changes in the solution. Such perturbations are impossible to find by simply changing the individual conductances, and the search space is very large if one were to search for combinations of changed conductances that give little effect on the action potential. The method is applicable for any model written on the standard form for action potential models; see Eqs. (5)–(6). The method is developed for investigating the sensitivity of the maximum conductances and it provides useful information about these parameters. The method is, however, not easy to generalize to all other adjustable parameters of AP models.

ACKNOWLEDGMENTS

This research was supported by the SUURPh (Simula—University of Oslo—UCSD) doctoral program, an international collaboration in computational biology and medicine funded by the Norwegian Ministry of Education and Research.

REFERENCES

[1]F. Dyson, "A meeting with Enrico Fermi," Nature **427**(6972), 297 (2004).
[2]A. L. Hodgkin and A. F. Huxley, "The components of membrane conductance in the giant axon of Loligo," J. Physiol. **116**(4), 473–496 (1952).
[3]D. Noble, "A modification of the Hodgkin–Huxley equations applicable to Purkinje fibre action and pacemaker potentials," J. Physiol. **160**(2), 317–352 (1962).
[4]See www.cellml.org/models/ for CellML Model Repository.
[5]G. B. Ermentrout and D. H. Terman, *Mathematical Foundations of Neuroscience* (Springer-Verlag, New York, 2010), Vol. 35
[6]D. Sterratt, B. Graham, A. Gillies, and D. Willshaw, *Principles of Computational Modelling in Neuroscience* (Cambridge University Press, 2011).
[7]R. Plonsey and R. C. Barr, *Bioelectricity, A Quantitative Approach* (Springer, 2007).
[8]J. P. Keener and J. Sneyd, *Mathematical Physiology* (Springer, 2009).
[9]F. H. Fenton and E. M. Cherry, "Models of cardiac cell," Scholarpedia **3**(8), 1868 (2008).
[10]Z. Qu, G. Hu, A. Garfinkel, and J. N. Weiss, "Nonlinear and stochastic dynamics in the heart," Phys. Rep. **543**(2), 61 (2014).
[11]Y. Rudy and J. R. Silva, "Computational biology in the study of cardiac ion channels and cell electrophysiology," Q. Rev. Biophys. **39**(01), 57–116 (2006).
[12]Y. Rudy, "From genes and molecules to organs and organisms: Heart," Comprehens. Biophys. **9**, 268–327 (2012).
[13]A. G. Edwards and W. E. Louch, "Species-dependent mechanisms of cardiac arrhythmia: A cellular focus," Clin. Med. Insights Cardiol. **11**, 1–14 (2017).
[14]S. A. Niederer, M. Fink, D. Noble, and N. P. Smith, "A meta-analysis of cardiac electrophysiology computational models," Exp. Physiol. **94**(5), 486–495 (2009).
[15]W. Groenendaal, F. A. Ortega, A. R. Kherlopian, A. C. Zygmunt, T. Krogh-Madsen, and D. J. Christini, "Cell-specific cardiac electrophysiology models," PLoS Comput. Biol. **11**(4), e1004242 (2015).
[16]S. D. Girouard, K. R. Laurita, and D. S. Rosenbaum, "Unique properties of cardiac action potentials recorded with voltage-sensitive dyes," J. Cardiovasc. Electrophysiol. **7**(11), 1024–1038 (1996).
[17]M. Canepari, D. Zecevic, and O. Bernus *et al.*, *Membrane Potential Imaging in the Nervous System and Heart* (Springer, 2015).
[18]K. Blinova, J. Stohlman, J. Vicente, D. Chan, L. Johannesen, M. P. Hortigon-Vinagre, V. Zamora, G. Smith, W. J. Crumb, L. Pang, B. Lyn-Cook, J. Ross, M. Brock, S. Chvatal, D. Millard, L. Galeotti, N. Stockbridge, and D. G. Strauss, "Comprehensive translational assessment of human-induced pluripotent stem cell derived cardiomyocytes for evaluating drug-induced arrhythmias," Toxicol. Sci. **155**(1), 234–247 (2017).
[19]A. Tveito, K. H. Jæger, N. Huebsch, B. Charrez, A. G. Edwards, S. Wall, and K. E. Healy, "Inversion and computational maturation of drug response using human stem cell derived cardiomyocytes in microphysiological systems," Sci. Rep. **8**(1), 17626 (2018).
[20]J. Liesen and V. Mehrmann, *Linear Algebra in Every Day Life* (Springer, 2015).
[21]T. Lyche, *Numerical Linear Algebra and Matrix Factorizations,* Lecture Notes (University of Oslo, 2017).
[22]M. T. Mora, J. M. Ferrero, L. Romero, and B. Trenor, "Sensitivity analysis revealing the effect of modulating ionic mechanisms on calcium dynamics in simulated human heart failure," PLoS One **12**(11), e0187739 (2017).
[23]M. Paci, J. Hyttinen, B. Rodriguez, and S. Severi, "Human induced pluripotent stem cell-derived versus adult cardiomyocytes: An in silico electrophysiological study on effects of ionic current block," Br. J. Pharmacol. **172**(21), 5147–5160 (2015).
[24]M. Paci, E. Passini, S. Severi, J. Hyttinen, and B. Rodriguez, "Phenotypic variability in LQT3 human induced pluripotent stem cell-derived cardiomyocytes and their response to anti-arrhythmic pharmacological therapy: An in silico approach," Heart Rhythm **14**, 1704–1712 (2017).
[25]B. Carbonell-Pascual, E. Godoy, A. Ferrer, L. Romero, and J. M. Ferrero, "Comparison between Hodgkin–Huxley and Markov formulations of cardiac ion channels," J. Theor. Biol. **399**, 92–102 (2016).
[26]H. W. J. Ten Tusscher and A. V. Panfilov, "Alternans and spiral breakup in a human ventricular tissue model," Am. J. Physiol. Heart Circulatory Physiol. **291**(3), H1088–H1100 (2006).
[27]E. Grandi, F. S. Pasqualini, and D. M. Bers, "A novel computational model of the human ventricular action potential and Ca transient," J. Mol. Cell. Cardiol. **48**(1), 112–121 (2010).
[28]T. O'Hara, L. Virág, A. Varró, and Y. Rudy, "Simulation of the undiseased human cardiac ventricular action potential: Model formulation and experimental validation," PLoS Comput. Biol. **7**(5), e1002061 (2011).
[29]R. H. Johnstone, E. T. Y. Chang, R. Bardenet, T. P. De Boer, D. J. Gavaghan, P. Pathmanathan, R. H. Clayton, and G. R. Mirams, "Uncertainty and variability in models of the cardiac action potential: Can we build trustworthy models?," J. Mol. Cell. Cardiol. **96**, 49–62 (2016).
[30]M. Fink and D. Noble, "Markov models for ion channels: Versatility versus identifiability and speed," Philos. Trans. R. Soc. A **367**(1896), 2161–2179 (2009).
[31]E. Marder and A. L. Taylor, "Multiple models to capture the variability in biological neurons and networks," Nat. Neurosci. **14**(2), 133 (2011).
[32]A. A. Prinz, D. Bucher, and E. Marder, "Similar network activity from disparate circuit parameters," Nat. Neurosci. **7**(12), 1345 (2004).
[33]P. Achard and E. De Schutter, "Complex parameter landscape for a complex neuron model," PLoS Comput. Biol. **2**(7), e94 (2006).
[34]A. X. Sarkar and E. A. Sobie, "Regression analysis for constraining free parameters in electrophysiological models of cardiac cells," PLoS Comput. Biol. **6**(9), e1000914 (2010).
[35]S. A. Mann, M. Imtiaz, A. Winbo, A. Rydberg, M. D. Perry, J.-P. Couderc, B. Polonsky, S. McNitt, W. Zareba, A. P. Hill, and J. I. Vandenberg, "Convergence of models of human ventricular myocyte electrophysiology after global optimization to recapitulate clinical long QT phenotypes," J. Mol. Cell. Cardiol. **100**, 25–34 (2016).
[36]S. Dokos and N. H. Lovell, "Parameter estimation in cardiac ionic models," Prog. Biophys. Mol. Biol. **85**(2–3), 407–431 (2004).
[37]J. Kaur, A. Nygren, and E. J. Vigmond, "Fitting membrane resistance along with action potential shape in cardiac myocytes improves convergence: Application of a multi-objective parallel genetic algorithm," PLoS One **9**(9), e107984 (2014).
[38]M. A. Herrera-Valdez and J. Lega, "Reduced models for the pacemaker dynamics of cardiac cells," J. Theor. Biol. **270**(1), 164–176 (2011).

[39]D. M. Lombardo and W.-J. Rappel, "Systematic reduction of a detailed atrial myocyte model," Chaos **27**(9), 093914 (2017).
[40]R. R. Aliev and A. V. Panfilov, "A simple two-variable model of cardiac excitation," Chaos Solitons Fractals **7**(3), 293–301 (1996).
[41]F. Fenton and A. Karma, "Vortex dynamics in three-dimensional continuous myocardium with fiber rotation: Filament instability and fibrillation," Chaos **8**(1), 20–47 (1998).
[42]S. K. Galappaththige, R. A. Gray, and B. J. Roth, "Cardiac strength-interval curves calculated using a bidomain tissue with a parsimonious ionic current," PLoS One **12**(2), e0171144 (2017).
[43]R. A. Gray and P. Pathmanathan, "A parsimonious model of the rabbit action potential elucidates the minimal physiological requirements for alternans and spiral wave breakup," PLoS Comput. Biol. **12**(10), e1005087 (2016).
[44]P. Kügler, A. H. Erhardt, and M. A. K. Bulelzai, "Early afterdepolarizations in cardiac action potentials as mixed mode oscillations due to a folded node singularity," PLoS One **13**(12), e0209498 (2018).
[45]G. Kerschen, J.-C. Golinval, A. F. Vakakis, and L. A. Bergman, "The method of proper orthogonal decomposition for dynamical characterization and order reduction of mechanical systems: An overview," Nonlinear Dyn. **41**(1–3), 147–169 (2005).
[46]C. W. Rowley, "Model reduction for fluids, using balanced proper orthogonal decomposition," Int. J. Bifurcat. Chaos **15**(03), 997–1013 (2005).
[47]E. A. Sobie, "Parameter sensitivity analysis in electrophysiological models using multivariable regression," Biophys. J. **96**(4), 1264–1274 (2009).
[48]A. X. Sarkar and E. A. Sobie, "Quantification of repolarization reserve to understand interpatient variability in the response to proarrhythmic drugs: A computational analysis," Heart Rhythm **8**(11), 1749–1755 (2011).
[49]A. X. Sarkar, D. J. Christini, and E. A. Sobie, "Exploiting mathematical models to illuminate electrophysiological variability between individuals," J. Physiol. (Lond.) **590**(11), 2555–2567 (2012).
[50]J. Q. X. Gong and E. A. Sobie, "Population-based mechanistic modeling allows for quantitative predictions of drug responses across cell types," NPJ Syst. Biol. Appl. **4**(1), 11 (2018).